Drag Effects on Wing Flutter

Augustin Petre*
Polytechnic Institute, Bucharest, Romania
and
Holt Ashley†
Stanford University, Stanford, Calif.

Using the large-aspect-ratio, cantilever wing as a model, the question is addressed as to whether forces of drag type may have a significant influence on dynamic aeroelastic stability. The elementary example of an elastically suspended "typical section" airfoil with constant drag and quasisteady airloads is analyzed first. Extensive flutter calculations then are carried out through numerical solution of the integral equations for a uniform wing with distributed properties in bending and torsion. Two-dimensional, incompressible unsteady theory for lifting airloads is combined with the assumption of a drag constant in magnitude and uniform across the wingspan. It is observed that, since drag never vanishes, some consideration always should be given to its influence on flutter and divergence. Tabulated results focus on the variation of critical speed and frequency with changes in a dimensionless drag parameter and a second parameter that associates bending rigidity, torsional rigidity, and aspect ratio. The effects of other key system parameters also are displayed. Even at low Mach number, it is found that this speed can be depressed by several percent below a purely potential-flow prediction when the aspect ratio is very large, whereas at intermediate aspect ratios it may be increased by a similar amount. Suggestions are made for further research on the phenomenon, notably for a study of supersonic flow where the drag parameter can have much higher values.

I. Introduction

By definition, aeroelastic phenomena involve mutual reciprocal interactions between the elastic and aerodynamic forces acting on a structure exposed to an airstream. They also are classified traditionally as dynamic or static, depending on whether or not inertia forces play a significant role. The accuracy with which aeroelastic behavior can be predicted (and in some cases even the theoretical existence of a particular class of instability or structural response) is related to the precision with which the various forces are expressed. It is, moreover, desirable that these levels of precision be consistent with one another. For example, suppose that a particular large-aspect-ratio lifting surface is idealized as one-dimensional structure, i.e., as one whose chordwise sections do not deform during bending and twisting. Then aerodynamic strip theory, with or without some approximate spanwise correction factor, often will suffice for estimating the airloads that it experiences.

Another hallowed aeroelastic tradition has been the primary concern with aerodynamic forces of lifting type, to the disregard of drag and chordwise force components generally. As will be seen in what follows, it can be argued that this neglect is unjustified and that it violates the test of consistency in circumstances that may arise in practice. The point is illustrated by previously published investigations of drag effects on static aeroelastic stability,[1,2,6] where hitherto unexpected phenomena were described due to the interaction of drag with deformations caused by lifting forces.

One interesting instance is the torsional divergence of an unswept, beam-rod wing when the distance between its aerodynamic and elastic centers is made to vanish. By the "classical" analysis, no static instability is predicted. With drag accounted for, however, a new instability appears wherein the drag works together with the lift and structural forces in quite a different fashion. Bending deformation now plays a part somewhat analogous to that of twisting in classical divergence. A full discussion of these results will be found in Ref. 1, pp. 449-487, and Goetz[2] has analyzed a similar case where a rigid lifting surface acts at the end of a beam-rod. Unlike lift and pitching moment, the drag never vanishes; hence it has been demonstrated that, when there is no sweepback, static aeroelastic instability is always a possibility.

The present paper addresses the question of whether drag ever may have a significant influence on dynamic aeroelastic stability, again using the large-aspect-ratio straight wing as a model. When one sets out to introduce the new force consistently into the equations of motion, the familiar tools of potential aerodynamic theory‡ fall down even under the simplifying assumption of strip theory. Lacking a wholly rational way to represent at least the viscous portion of drag and seeking an approximation that properly characterizes the phenomenon without undue complexity, one is faced with a choice between alternatives: 1) either lift and drag may be employed, in the classical manner, as forces with fixed directions relative to the freestream, and this hypothesis may be carried over to the case of periodic displacements and rotations; or 2) the two force components may be attached to the airfoil like a follower system, with one part dependent on the angle of attack and (for example) a component in the chord plane which is assumed constant. It is noted that the latter scheme accords

Received May 23, 1975; presented as Paper 75-775 at the AIAA/ASME/SAE 16th Structures, Structural Dynamics, and Materials Conference, Denver, Colo., May 27-29, 1975; revision received Dec. 18, 1975. This research was supported in part by the Air Force Office of Scientific Research, Contract AFOSR 74-2712, and in part under the Cooperative Science Program administered between the U.S. National Science Foundation and the Romanian National Council for Science and Technology. The NSF Grant to Stanford University is GK 35004.

Index categories: Aeroelasticity and Hydroelasticity; Aircraft Vibration.

*Professor and Head, Department of Aeronautical Engineering.

†Professor, Aeronautics and Astronautics. Honorary Fellow AIAA.

‡These are summarized, among other places, in Chap. 4 of Ref. 3. It is worth mentioning that Wagner[4] has discussed how steady three-dimensional lifting-surface theory may be used to find spanwise distributions of both the induced drag and leading-edge suction force. There are fairly obvious possibilities of extending his results to oscillatory motion along lines laid down by Garrick[5] for the two-dimensional case, but of course the viscous contributions to unsteady drag are quite another question.

quite well with measurements on many profiles through a limited range of incidence in steady, subsonic flow.

Choosing the former representation, Petre[6] first analyzed drag effects on wing flutter by the method of assumed modes. He discovered an extreme sensitivity of the predicted eigenvalues to the particular choice of bending and torsion mode shapes. It therefore appears desirable to re-examine the problem in a way that exerts less constraint upon the mode at flutter.

The follower-force approach also has been employed[7] but only in a very special application, where a concentrated chord force at the wingtip was intended to idealize propulsive thrust during vertical takeoff. Here the method of fixed directions is selected. The wing is an unswept cantilever of constant cross section. Strip theory for incompressible unsteady flow is adopted as a source of loads in the lift direction, whereas drag is assumed to have invariant direction and magnitude all across the span.

In order to clarify the physical phenomenon, an elementary example will be treated first: the "typical section" airfoil with elastically restrained freedoms in pitch and plunge under stationary aerodynamic forces. The major portion of the paper then is devoted to a cantilever with distributed elastic properties and unsteady airloads of strip type.

II. Typical Section Wing

Figure 1 illustrates the rigid, two-dimensional wing, suspended by a pair of springs in a rather artificial fashion that simulates the way in which bending displacement of an elastic cantilever can interact with the drag force to produce twisting at stations inboard of where each element of drag acts. The wing is constrained to two degrees of freedom by a massless, pivoted bar that slides in a bushing or slide-bearing passing through the wing c.g. The "bending" freedom w is the distance along this bar from the pivot to the c.g., whereas "torsion" is represented by the *small* angle φ by which the bar and wing are rotated clockwise from the zero-angle-of-attack position. A second constraining bar, extensible but rigid in bending like a spline and located a distance e_1c ahead of the first, connects a pair of pivots at ground and at the simulated elastic axis (E.C.). The latter bar is acted upon by a torsion spring, constant K_φ, restraining it about the lower pivot; a linear spring, constant K_w, acts along this bar between the pivot and the E.C. This arrangement produces an instantaneous pivot torque and a force at the elastic center with magnitudes, respectively,

$$F_\varphi = K_\varphi \varphi, \qquad F_w = K_w[w + e_1 c\varphi] \tag{1}$$

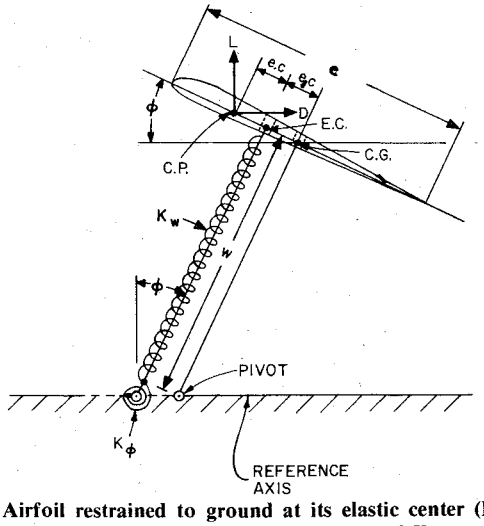

Fig. 1 Airfoil restrained to ground at its elastic center (E.C.) by flexural and torsional springs with constants K_w and K_φ, respectively. The airstream is directed horizontally with dynamic pressure q. Directions of lift L and drag D are fixed through the center of pressure (C.P.).

The equations of motion for this system are derived best by Lagrange's procedure. It then is found, for instance, that this particular choice of degrees of freedom yields a kinetic energy, to second order in w, φ,

$$\tfrac{1}{2}[M\dot{w}^2 + J_G\dot{\varphi}^2]$$

so that no inertial coupling exists. Unsteady effects, structural and aerodynamic damping are neglected, in the manner suggested by Pines.[8] Also omitted in the bending equation is a very small force associated with the drag.

The equations of motion under steady airloads read§

$$M\ddot{w} + K_w[w + e_1 c\varphi] = qS(dC_L/d\alpha)\varphi$$

$$J_G\ddot{\varphi} = K_\varphi\varphi + K_w[w + e_1 c\varphi]e_1 c = qS(dC_L/d\alpha)[e + e_1]c\varphi + qSC_D[w + (e + e_1)c\varphi] \tag{2}$$

At the flutter stability boundary, w and φ will have simple-harmonic time dependence with frequency ω and amplitudes W and Φ:

$$W\left[-\omega^2 + \frac{K_w}{M}\right] + \Phi\left[\frac{K_w e_1 c}{M} - \frac{qS}{M}\frac{dC_L}{d\alpha}\right] = 0 \tag{3a}$$

$$W\left[\frac{K_w}{J_G}e_1 c - \frac{qSC_D}{J_G}\right] + \Phi\left[-\omega^2 + \frac{K_\varphi}{J_G} + \frac{K_w e_1^2 c^2}{J_G} - \frac{qS}{J_G}\frac{dC_L}{d\alpha}(e + e_1)c - \frac{qSC_D}{J_G}(e + e_1)c\right] = 0 \tag{3b}$$

The characteristic equation of (3) is

$$\left[\omega^2 - \frac{K_w}{M}\right]\left[\omega^2 - \frac{K_\varphi}{J_G}\right] - \omega^2\left[\frac{K_w}{J_G}e_1^2 c^2 - \frac{qS}{J_G}\left(\frac{dC_L}{d\alpha} + C_D\right)(e + e_1)c\right] + \frac{K_w}{M}\frac{qS}{J_G}\left(\frac{dC_L}{d\alpha} + C_D\right)e - \frac{q^2S^2}{J_G M}C_D\frac{dC_L}{d\alpha} = 0 \tag{4}$$

A convenient dimensionless form of (4) reads

$$(X - B_1)(X - 1) - X[(B_1/B_2)e_1^2 - Y(e + e_1)(1 + C)] - YB_1 e(1 + C) - Y^2 B_2 C = 0 \tag{5}$$

with the following parameters:

$$X = (J_G\omega^2/K_\varphi) = (\omega^2/\omega_\varphi^2) \tag{6a}$$

$$Y = (qSc/K_\varphi)(dC_L/d\alpha) \tag{6b}$$

$$B_1 = (\omega_w^2/\omega_\varphi^2) \equiv (K_w/M)/(K_\varphi/J_G) \tag{6c}$$

$$B_2 = (J_G/Mc^2) \tag{6d}$$

$$C = [C_D/(dC_L/d\alpha)] \tag{6e}$$

All terms except the first in (4) and (5) describe various couplings, either elastic or aerodynamic. The drag is seen to act in two ways. The first involves a direct increase in lift-curve slope through the factors containing $(1 + C)$. Because $C \ll 1$ in most designs, this is quantitatively a small effect, does not change the structure of the equations, and probably could be neglected. The second influence of drag is more complicated, since a term containing the square of the aerodynamic parameter Y is introduced.

§Standard aerodynamic notation is used, with the exception that φ (rather than θ or α) is the angle of pitch. The only other symbols not defined in Fig. 1 are wing mass M and c.m. moment of inertia J_G.

A graphical scheme is available which assists with the understanding of this example. If drag is omitted ($C=0$), (5) plots in the X-Y coordinates as a hyperbola, one of whose legs has its asymptote parallel to the Y axis. Figure 2 illustrates the situation for a particular choice of system parameters. It is of interest that this asymptote's distance from the Y axis is proportional to the quantity e, which measures how far the elastic center is behind the aerodynamic center. When drag is included in (5), as shown by dashed lines in Fig. 2 for $C=0.06$, the solution is again a hyperbola but with its center displaced and axes rotated relative to the same wing at $C=0$.

It is worth adding that the Fig. 2 curves depict the roots of (5) only for those parametric ranges where they are real. That is, for $C=0$, one observes that there is a range of Y (or of dynamic pressure q for a given wing) between Y_F and $Y_{F'}$ where X is neither a positive or negative real number. Within this range X, and therefore the square of frequency ω, must occur as a complex-conjugate pair. It follows that one of the corresponding vibration-mode envelopes will be exponentially divergent in time and that the system is unstable within the linear range. There is a nonoscillatory instability whenever X is real and negative.

The characteristic hyperbola has a center with the following coordinates:

$$X_0=\frac{1}{2}\left[1+B_1+\frac{B_1}{B_2}e_1^2\right] - \frac{\left[\frac{1}{2}\left(1+B_1+\frac{B_1}{B_2}e_1^2\right)-B_1e/(e+e_1)\right]}{\frac{4B_2C}{[e+e_1]^2[1+C]^2}+1} \tag{7a}$$

$$Y_0=\frac{\left[\frac{1}{2}\left(1+B_1+\frac{B_1}{B_2}e_1^2\right)(e+e_1)(1+C)-B_1e(1+C)\right]}{2B_2C+\frac{1}{2}[e+e_1]^2[1+C]^2} \tag{7b}$$

As drag parameter C increases, one can show that X_0 increases and Y_0 decreases. The asymptotes intersecting at center X_0, Y_0 have slopes as follows:

$$\lim\left(\frac{Y}{X}\right)_\infty=\begin{cases} -\dfrac{1}{[e+e_1][1+C]} \\ \dfrac{1}{[e+e_1][1+C]}+\dfrac{[e+e_1][1+C]}{B_2C} \end{cases} \tag{8}$$

The second asymptote here is evidently the one that parallels the Y axis at $C=0$; its slope is positive for the usual case of $[e+e_1]>0$ and decreases as drag C increases. The other asymptote has a negative slope, whose magnitude is reduced slightly by increasing C.

Some further comments are offered about the physical significance of the foregoing construction. One obvious limiting case is when the aerodynamic forces vanish at zero dynamic pressure ($Y=0$). The system then can execute coupled, undamped vibrations with natural frequencies determinable from the two roots of (5):

$$X_{1,2}=\frac{1}{2}\left\{1+B_1+e_1\mp\left[\left(1+B_1+\frac{B_1}{B_2}e_1^2\right)^2-4B_1\right]^{1/2}\right\} \tag{9}$$

Given appropriate initial conditions, the displacements and rotations may be determined vs time as superpositions of simple harmonic oscillations.

In the absence of elastic coupling ($e_1=0$), the $Y=0$ eigenvalues become

$$\bar{X}_{1,2}=B_1,1 \tag{10}$$

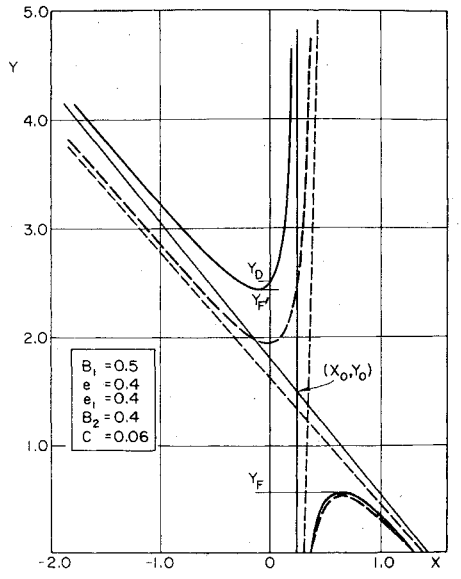

Fig. 2 Real roots of characteristic equation (5) for drag parameters $C=0$ (solid lines) and $C=0.06$ (dashed lines). Also indicated are the asymptotes for the two pairs of hyperbolas. (Note that the point X_0, Y_0 and the ordinates Y_F, etc., are marked for the case $C=0$ only.)

It easily is observed that

$$X_1<(B_1,1)<X_2 \tag{11}$$

i.e., the well-known separation of the frequencies due to the addition of coupling is confirmed.

As Y is increased from zero, the system is found to possess two distinct real frequencies in a zone $0\le Y<Y_F$. A frequency merging (cf. Fig. 2) at $Y=Y_F$ corresponds to the lower q boundary for flutter instability. The dynamic pressure or speed associated therewith can be calculated from

$$Y_F=\left\{(e_1+e+eC)(X_1+X_2)-2B_1[e+(e-e_1)C]\cdot \cdot\left[1-\left(\frac{[(e_1+e+eC)^2+4B_2C](X_1-X_2)^2}{[e_1+e+eC)(X_1+X_2)-2B_1(e+eC-e_1C)]^2}\right)^{1/2}\right]\right\} \Big/ [(e_1+e+eC)^2+4B_2C] \tag{12}$$

The corresponding dimensionless frequency parameter is

$$X_F=\frac{1}{2}\left[1+B_1+\frac{B_2}{B_1}e_1^2-Y_F(e+e_1)(1+C)\right] \tag{13}$$

It can, incidently, be shown that nonlinear effects are present which ultimately would limit the growth of this mode. One also can see that increasing drag generally reduces the critical flutter speed when other parameters remain unchanged.

Another significant point in Fig. 2 occurs at $Y=Y_D$, where $X=0$. It represents a critical divergence speed but not a "stability boundary" in the conventional sense, because of the peculiar behavior of the eigenvalues as functions of Y for this particular system. From (5), it can be deduced that for zero drag

$$Y_D=1/e \tag{14}$$

whereas for $C>0$

$$Y_D=\frac{1}{2B_2C}\{-B_1[e+(e-e_1)C] +(B_1^2[e+(e-e_1)C]^2+4B_1B_2C)^{1/2}\} \tag{15}$$

Equations (14) and (15) demonstrate that, when $e \to 0$ at $C=0$ and the vertical asymptote coincides with the Y axis, the divergence phenomenon is predicted to disappear. Drag is never zero in actuality, however, and so there always will be an intersection between the hyperbola and the Y axis. Hence divergence never entirely vanishes.

To summarize, there exist four important ranges of parameter Y, within each of which it is instructive to examine the distinct character of the motions that can take place there:

$$\begin{array}{ll} 1)\ 0 \le Y \le Y_F & 3)\ Y_{F'} \le Y \le Y_D \\ 2)\ Y_F < Y < Y_{F'} & 4)\ Y_D < Y \end{array} \qquad (16)$$

III. Bending-Torsion Flutter of a Straight Uniform Cantilever Wing

Several different operators are available for defining the elastic forces and thus for setting up the equations of the one-dimensional structure. In what follows, a progression will be made from differential to integral to matrix forms of these operators. As discussed previously, aerodynamic operators of strip type will be adapted from unsteady, incompressible flow theory (cf. pp. 104-106 of Ref. 3). Lift and drag will be assumed to have fixed directions relative to the freestream, and indeed the running drag will be taken as a constant across the wingspan.

This assumption on drag implies, at the very least, that the elastic deformations $\varphi(y,t)$ in torsion and $w(y,t)$ in flexure always must remain small. y and t denote, respectively, a spanwise coordinate along the straight line of elastic centers and time. The initial position of the wing is at zero angle of attack.

Experience[2] suggests that methods relying upon the assumption of a few prescribed deformation modes should be avoided. Accordingly, the ultimate solution for flutter modes and eigenvalues will employ here a matrix scheme based on collocation of the governing integral equations. The possibility of structural damping will be introduced by means of a complex elastic modulus: the familiar "V-g method" (p. 381, Ref. 3).

As adapted from the steady-motion derivation given after p. 449 of Petre's book,[1] the differential equations of bending and torsion are

$$\frac{\partial^2}{\partial y^2}\left[(1+ig_w)EI\frac{\partial^2 w}{\partial y^2}\right] + m\frac{\partial^2 w}{\partial t^2} + s\frac{\partial^2 \varphi}{\partial t^2} - L_a(w,\psi) + \frac{\partial^2}{\partial y^2}(M_z\varphi) = 0 \qquad (17a)$$

$$\frac{\partial}{\partial y}\left[(1+ig_\varphi)GI_d\frac{\partial \varphi}{\partial y}\right] - J\frac{\partial^2 \varphi}{\partial t^2} - s\frac{\partial^2 w}{\partial t^2} + m_a(w,\varphi) - M_z\frac{\partial^2 w}{\partial y^2} = 0 \qquad (17b)$$

All forms and notation in (17) are generally well known to aeroelasticians with the exception of the factors M_z, which embody the drag airloads. The first term in each equation represents elastic forces expressed by differential operators, the small quantities g_w and g_φ being the respective structural-damping coefficients; the second term represents a direct inertia force; the third is an inertia coupling force; the forth is an implicit form of the lifting airloads; and the last contains effects of drag. Evidently, each term in (17a) amounts to a force per unit spanwise distance, whereas the (17b) involves a sum of moments per unit span.

For simple harmonic motion of circular frequency ω, the strip-theory aerodynamic force and moment are [cf. (4-123) and (4-124) of Ref. 3]

$$L_a(w,\varphi) = \pi\rho b^3\omega^2\{L_w(w/b) + [L_\varphi - (\tfrac{1}{2}+a)L_w]\varphi\} \qquad (18a)$$

$$m_a(w,\varphi) = \pi\rho b^4\omega^2\{[M_w - (\tfrac{1}{2}+a)L_w](w/b) + [M_\varphi - (\tfrac{1}{2}+a)(L_\varphi + M_w) + (\tfrac{1}{2}+a)^2 L_w]\varphi\} \qquad (18b)$$

where

$$L_w = 1 - 2i(V/b\omega)(F_k + iG_k) \qquad (19a)$$

$$L_\varphi = \tfrac{1}{2} - i(V/b\omega)[1 + 2(F_k + iG_k)] - 2(V/b\omega)^2(F_k + iG_k) \qquad (19b)$$

$$M_w = \tfrac{1}{2} \qquad (19c)$$

$$M_\varphi = (3/8) - i(V/b\omega) \qquad (19d)$$

Here, V, ρ, and b are airspeed, density, and wing semichord, respectively; a is the distance in semichords by which the elastic centers lie aft of the midchord line. F_k and G_k are the familiar Theodorsen functions of reduced frequency $k \equiv \omega b/V$.

As developed in Refs. 1 and 6, bending moment M_z is associated with the uniform running drag. Its value in the present case can be written as follows in terms of the constant aerodynamic coefficient C_D:

$$M_z = (\rho/2)V^2 C_D \tfrac{1}{2}[\ell - y]^2 2b \qquad (20)$$

where ℓ is the root-to-tip distance, equivalent to wing semispan.

The customary assumption of simple harmonic motion is made in order to calculate stability boundaries. With $w(y)$ and $\varphi(y)$ the dimensionless flutter modal displacements and W_0, Φ_0 reference amplitudes, one which may be unity, there are thus obtained

$$w(y,t) = W_0 w(y) e^{i\omega t}, \quad \varphi(y,t) = \Phi_0 \varphi(y) e^{i\omega t} \qquad (21)$$

When (18-21) are substituted into (17) and the resulting equations are nondimensionalized, the usual profusion of new notation appears. Since it will be a question of calculating complex eigenvalues, the simplest way of summarizing the situation is to state that the unknown velocity and frequency parameters¶

$$X = V/b\omega \qquad (22)$$

$$Z = [1+ig](GI_d/J\ell^2\omega^2) \qquad (23)$$

are to be determined as functions of the following six dimensionless quantities, all of which may be specified in advance for incompressible flow past a uniform wing:

$$M = (m/\pi\rho b^2) \qquad (24a)$$

$$i_\alpha = (J/mb^2) \qquad (24b)$$

$$A = \tfrac{1}{2} + a \qquad (24c)$$

$$S = s/bm \qquad (24d)$$

$$p = (EIb^2/GI_d\ell^2) \qquad (24e)$$

$$C = (C_D/(dC_L/d\alpha) \qquad (24f)$$

¶Here the usual approximation $g_w = g_\varphi = g$ is adopted.

The actual calculation process starts from dimensionless differential equations in the form

$$W_0\frac{d^4w(y)}{dy^4}-[(A_1+iA_2)W_0w(y)+(A_3+iA_4)\Phi_0\varphi(y)]\frac{1}{Z}$$

$$-\Phi_0A_9\frac{1}{Z}\frac{d^2}{dy^2}[(1-y)^2\varphi(y)]=0 \tag{25a}$$

$$\Phi_0\frac{d^2\varphi(y)}{dy^2}+[(A_5+iA_6)W_0w(y)+(A_7+iA_8)\Phi_0\varphi(y)]\frac{1}{Z}$$

$$+W_0A_{10}\frac{1}{Z}\frac{d^2w(y)}{dy^2}=0 \tag{25b}$$

where

$$A_1=\frac{1}{pi_\alpha}\left[1+\frac{1}{M}(1+2X\cdot G_k)\right] \tag{26a}$$

$$A_2=-\frac{2}{pMi_\alpha}X\cdot F_k \tag{26b}$$

$$A_3=\frac{1}{pi_\alpha}\left\{S+\frac{1}{M}[\tfrac{1}{2}+2X\cdot G_k-2X^2F_k-A(1+2X\cdot G_k)]\right\} \tag{26c}$$

$$A_4=\frac{1}{pMi_\alpha}[2A\cdot F_k-1-2F_k-2X\cdot G_k]X \tag{26d}$$

$$A_5=\frac{1}{i_\alpha}\left\{S+\frac{1}{M}[\tfrac{1}{2}-A(1+2X\cdot G_k)]\right\} \tag{26e}$$

$$A_6=\frac{2}{Mi_\alpha}A\cdot X\cdot F_k \tag{26f}$$

$$A_7=1+\frac{1}{Mi_\alpha}[0.375-A(1+2X\cdot G_k-2X^2\cdot F_k)$$

$$+A^2(1+2A\cdot G_k)] \tag{26g}$$

$$A_8=\frac{1}{Mi_\alpha}[-1+A(1+2F_k+2X\cdot G_k)-2A^2\cdot F_k]X \tag{26h}$$

$$A_9=\frac{C}{pMi_\alpha}X^2 \tag{26i}$$

$$A_{10}=\frac{C}{Mi_\alpha}X^2 \tag{26j}$$

In (25), y has been rendered dimensionless by division with ℓ.

The boundary conditions associated with (25) involve built-in cantilever restraints at the root $y=0$ and zero torque, shear and bending moment at the free tip $y=1$. After considerable effort, it has been shown that the following pair of integral equations is equivalent to (25), together with the six prescribed conditions:

$$W_0w(y)=\frac{1}{Z}\left\{\int_0^y\frac{\eta^2}{6}(3y-\eta)[A_1+iA_2)W_0w(\eta)\right.$$

$$+(A_3+iA_4)\Phi_0\varphi(\eta)]d\eta+\int_y^1\frac{y^2}{6}(3\eta-y)[(A_1+iA_2)W_0w(\eta)$$

$$+(A_3+iA_4)\Phi_0\varphi(\eta)]d\eta$$

$$\left.+A_9\int_0^y(y-\eta)(1-\eta)^2\Phi_0\varphi(\eta)d\eta\right\} \tag{27a}$$

$$\Phi_0\varphi(y)=\frac{1}{Z}\left\{\int_0^y\eta[(A_5+iA_6)W_0w(\eta)+(A_7+iA_8)\Phi_0\varphi(\eta)]d\eta\right.$$

$$+\int_y^1y[A_5+iA_6)W_0w(\eta)+(A_7+iA_8)\Phi_0\varphi(\eta)d\eta$$

$$\left.+A_{10}\left[\int_0^y(3\eta-2)W_0w(\eta)d\eta+\int_y^1yW_0w(\eta)d\eta\right.\right.$$

$$\left.\left.-\frac{(1-y)^2}{2}W_0w(y)\right]\right\} \tag{27b}$$

It can be seen that four types of integral operators occur in these equations. Two are the conventional Green's functions for bending and torsion of the cantilever. The others are the two that are multiplied by the drag parameters A_9 and A_{10}. They respectively embody the drag effects on bending and on torsion, as these effects appear in the final terms of (17). It is convenient to abbreviate these four operators by the symbols G_w, G_φ, D_w, and D_φ.

The complex mode shapes $w(y)$, $\varphi(y)$ are next replaced by normalized vectors $\{w\}$, $\{\varphi\}$ containing their values at n equally spaced stations across the wingspan. Let the two equations (27) be divided by W_0 and Φ_0, and introduce a suitable numerical integration formula so that all integrands can be approximated in terms of values at the points chosen for collocation. There results a system of $2n$ homogeneous algebraic equations, with the $2n$ complex modal-vector components as unknowns, in the following forms

$$\{w\}=(1/Z)\{(A_1+iA_2)[G_w]\{w\}+\langle(A_3+iA_4)[G_w]\{\varphi\}$$

$$+A_9[D_w]\{\varphi\}\rangle(\Phi_0/W_0) \tag{28a}$$

$$\{\varphi\}=(1/Z)\{\langle(A_5+iA_6)[G_\varphi]\{w\}+A_{10}[D_\varphi]\{w\}\rangle$$

$$\times(W_0/\Phi_0)+(A_7+iA_8)[G_\phi]\{\varphi\}\} \tag{28b}$$

Here the bracketed quantities are obviously $n\times n$ square matrices containing values of the four Green's functions multiplied by weighted coefficients arising from the quadrature formula.

There are many ways in which a system like (28) can be solved for its complex eigenvectors and eigenvalues. One that has proved efficient for the present case consists of the following steps:

1) Suitable initial approximations are made for the vectors $\{w\}$ and $\{\varphi\}$, e.g., with values of unity at the wingtip station. This means that the phase difference in the flutter mode at the tip is carried by the ratio W_0/Φ_0.

2) With $w_n=1+i\times0$ and $\varphi_n=1+i\times0$, the various matrix products in (28), which now are composed of known quantities, may be evaluated.

3) The approximations to (28) are set up for the wingtip station only and manipulated into a complex quadratic equation for Z by eliminating the ratio W_0/Φ_0. The latter can be solved for Z except that the A_i appearing in the solution depend in an elaborate way on the reduced velocity X,

4) Since

$$\frac{\mathrm{Im}(Z)}{\mathrm{Re}(Z)}=g \tag{29}$$

it is possible by repeated trials to determine one or more (real) values of X which correspond to the prescribed value of this structural-damping parameter. Thus first-approximate pairs of the eigenvalues X and Z can be calculated, to each of which corresponds a ratio Φ_0/W_0 and a wingtip phase angle δ, such that

$$\tan\delta=\frac{\mathrm{Im}(\Phi_0/W_0)}{\mathrm{Re}(\Phi_0/W_0)} \tag{30}$$

Table 1 Dimensionless flutter and divergence eigenvalues as functions of the system parameters

p	M	i_α	S	A	g	C	$\frac{V\ell}{b}\sqrt{\frac{J}{GI_d}}$	$\omega\ell\sqrt{\frac{J}{GI_d}}$	tan δ	$\frac{V_D\ell}{b}\sqrt{\frac{J}{GI_d}}$
						0.00	4.032	0.886	-0.875	5.55
0.004	10	0.25	0.1	0.1	0.0	0.02	3.953	0.919	-0.759	2.33
						0.04	3.993	0.930	-0.740	1.98
						0.00	5.268	0.882	-0.507	
0.004	20	0.25	0.1	0.1	0.0	0.02	5.082	0.923	-0.468	
						0.04	5.056	0.937	-0.449	
						0.00	7.127	0.875	-0.324	11.1
0.004	40	0.25	0.1	0.1	0.0	0.02	6.797	0.919	-0.295	4.66
						0.04	6.715	0.934	-0.279	3.96
						0.00	10.876	0.858	-0.177	
0.004	100	0.25	0.1	0.1	0.0	0.02	10.277	0.903	-0.156	
						0.04	10.105	0.916	-0.144	
						0.00	9.914	0.889	-0.463	∞
0.004	40	0.25	0.1	0.0	0.0	0.02	8.984	0.975	-0.357	4.895
						0.04	8.925	0.994	-0.324	4.100
						0.00	5.918	0.865	-0.265	
0.004	40	0.25	0.1	0.2	0.0	0.02	5.750	0.894	-0.253	
						0.04	5.699	0.904	-0.246	
						0.00	7.084	0.907	-0.338	∞
0.004	40	0.25	0.2	0.0	0.0	0.02	6.865	0.941	-0.370	4.895
						0.04	6.837	0.952	-0.296	4.104
						0.00	5.923	0.892	-0.281	
0.004	40	0.25	0.2	0.1	0.0	0.02	5.818	0.912	-0.271	
						0.04	5.800	0.920	-0.264	
						0.00	7.238	0.855	-0.337	
0.004	40	0.25	0.1	0.1	0.02	0.02	6.876	0.906	-0.304	
						0.04	6.790	0.923	-0.287	
						0.00	7.901	0.990	-0.324	
0.004	40	0.35	0.1	0.1	0.0	0.02	7.419	1.041	-0.295	
						0.04	7.287	1.057	-0.279	
0.04	10	0.25	0.1	0.1	0	0.00	4.070	0.903	-0.909	
						0.02	4.510	0.910		
						0	5.274	0.889	-0.569	
0.04	20	0.25	0.1	0.1	0	0.02	5.68	0.896	-0.588	
						0.04	6.534	0.909		
						0	7.159	0.870	-0.364	
0.04	40	0.25	0.1	0.1	0	0.02	7.647	0.878	-0.379	
						0.04	8.521	0.892	-0.404	
						0	11.039	0.829	-0.204	
0.04	100	0.25	0.1	0.1	0	0.02	11.798	0.847	-0.215	
						0.04	13.071	0.858		
0.04	40	0.25	0.1	0	0	0.00	9.872	0.898	-0.493	
						0	5.958	0.853	-0.303	
0.04	40	0.25	0.1	0.2	0	0.02	6.123	0.857	-0.309	
						0.04	6.324	0.860	-0.315	
						0	4.767	0.820	-0.236	
0.04	40	0.25	0.1	0.4	0	0.02	4.814	0.822	-0.238	
						0.04	4.863	0.824	-0.239	
						0	7.145	0.898	-0.362	∞
0.04	40	0.25	0.2	0	0	0.02	7.522	0.904	-0.373	8.70
						0.04	8.102	0.912	-0.390	7.30
						0	5.985	0.877	-0.311	
0.04	40	0.25	0.2	0.1	0	0.02	6.118	0.879	-0.315	
						0.04	6.275	0.880	-0.320	
						0	5.286	0.859	-0.277	
0.04	40	0.25	0.2	0.2	0	0.02	5.350	0.859	-0.279	
						0.04	5.420	0.860	-0.281	
0.04	40	0.25	0.1	0.1	0.02	0	7.235	0.851	-0.383	
						0.02	7.771	0.861	-0.400	
						0	7.924	0.978	-0.370	
0.04	40	0.35	0.1	0.1	0	0.02	8.440	0.984	-0.386	
						0.04	9.378	0.996	-0.413	

TABLE 1 (continued)

p	M	i_α	S	A	g	C	$\frac{V\ell}{b}\sqrt{\frac{J}{GI_d}}$	$\omega\ell\sqrt{\frac{J}{GI_d}}$	tan δ
						0	2.699	1.309	-0.300
0.4	10	0.25	0.1	0.1	0	0.02	2.753	1.305	-0.292
						0.04	2.823	1.300	-0.284
						0	3.220	1.307	-1.451
0.4	20	0.25	0.1	0.1	0	0.02	3.245	1.304	-1.431
						0.04	3.275	1.301	-1.412
						0	4.155	1.296	-0.812
0.4	40	0.25	0.1	0.1	0	0.02	4.176	1.294	-0.806
						0.04	4.199	1.293	-0.800
						0	6.082	1.274	-0.412
0.4	100	0.25	0.1	0.1	0	0.02	6.108	1.273	-0.411
						0.04	6.136	1.273	-0.410
						0	4.664	1.295	-0.820
0.4	40	0.25	0.1	0	0	0.02	4.713	1.293	-0.818
						0.04	4.772	1.291	-0.817
						0	3.795	1.297	-0.825
0.4	40	0.25	0.1	0.2	0	0.02	3.805	1.295	-0.816
						0.04	3.816	1.294	-0.808
						0	3.312	1.293	-0.879
0.4	40	0.25	0.1	0.4	0	0.02	3.314	1.292	-0.867
						0.04	3.315	1.292	-0.855
						0	4.388	1.354	-1.041
0.4	40	0.25	0.2	0	0	0.02	4.383	1.352	-1.027
						0.04	4.378	1.350	-1.014
						0	4.085	1.348	-1.241
0.4	40	0.25	0.2	0.1	0	0.02	4.078	1.347	-1.220
						0.04	4.071	1.345	-1.200
						0	3.850	1.339	-1.538
0.4	40	0.25	0.2	0.2	0	0.02	3.842	1.338	-1.505
						0.04	3.835	1.337	-1.474
						0	4.246	1.290	-0.897
0.4	40	0.25	0.1	0.1	0.02	0.02	4.271	1.288	-0.892
						0.04	4.300	1.287	-0.887
						0	3.535	1.466	-1.822
0.4	40	0.35	0.1	0.1	0	0.02	3.537	1.464	-1.778
						0.04	3.540	1.463	-1.737

5) Returning to (28), one sees that a first approximation has been found for all quantities appearing in their right-hand sides. In the manner of Stodola and Vianello, Eqs. (28) then are employed to calculate a second (complex) approximation to the eigenvectors $\{w\}$ and $\{\varphi\}$. These are again normalized to unity tip values.

6) With second, improved estimates of the eigenvectors, the entire process is repeated from step 1. The iteration proceeds until two successive values of a preselected control variable differ by less than a prescribed amount. In the results given below, Z was used as this control. The imposed precision called for convergence in its magnitude to $\leq 0.001\%$. No difficulties have been encountered in practice with this scheme. An alternative scheme for determining these solutions is the direct calculation of the roots of the determinant of linear system (28), with $\{\Phi_0\varphi; W_0 w\}$ as the vector of generalized coordinates. Although more expensive in computer time, this approach has been employed to check all results for $p=0.004$ in Table 1. To five significant figures, identical numbers generally are obtained.

IV. Presentation and Discussion of Results for the Cantilever Wing

Numerous flutter calculations have been carried out, with incompressible strip theory, for practical ranges of the six parameters in (24) and two values of structural damping g. Table 1 contains a selection of the resulting eigenvalues expressed in terms of the dimensionless critical speed $(V\ell/b)(J/GI_d)^{1/2}$ and frequency $\omega\ell(J/GI_d)^{1/2}$. Also listed is the tangent of the phase angle δ by which torsional displacement at the wingtip leads bending displacement in the flutter mode.

The two independent parameters regarded as the most interesting from the standpoint of this study are p and C. p is seen from (24) to be the ratio of bending rigidity to torsional rigidity (a number that is rather insensitive to property variations from one large-aspect-ratio wing to another and ranges between 1 and 2) multiplied by the inverse square of ℓ/b. The latter ratio is approximately the aspect ratio of the full-span wing equivalent to the cantilever structure analyzed here. Hence p ranging from 0.004 to 0.4 covers aspect ratios roughly from 20 down to 2, the latter number being so low as to invalidate the theory. C is the drag coefficient referenced to sectional lift curve slope. Since $dC_L/d\alpha$ runs 5-6 and the (profile plus induced) drag of many subsonic wings is in the vicinity of $C_D=0.02$, it will be noted that the values 0.02 and 0.04 chosen for C are on the high side. This is done intentionally, so as to magnify the drag effect.

It is worth mentioning that parallel calculations of flutter speed and frequency were conducted under the assumption that the modal vectors $\{w\}$ and $\{\varphi\}$ were purely real, prior to introducing the complex vectors that permit phase differences between various spanwise stations. As a rule, with all other parameters the same, it was found that the two sets of eigenvalues differed by less than 1%. As might be anticipated, the

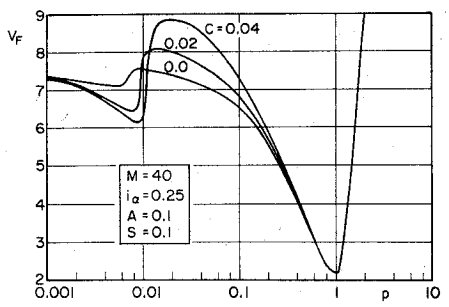

Fig. 3 Variation of dimensionless flutter speed $V_F \equiv (V\ell/b)(J/GI_d)^{1/2}$ with an aspect-ratio parameter p, plotted for three values of drag parameter C.

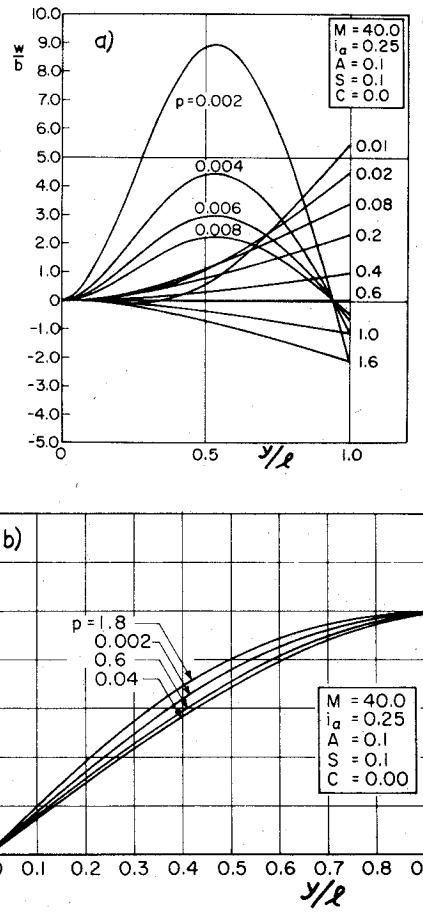

Fig. 4 a) Bending and b) torsional flutter mode shapes, plotted vs dimensionless spanwise distance for zero drag. Small differences in phase between spanwise stations within each modal component are neglected. Refer to Table 1 for typical values of the phase angle δ between bending and torsion at the wingtip.

bending oscillation tended to occur in phase within 2° or 3° across the span, and the torsion did as well.

For values of $p=0.04$ and greater, the number of collocation points in the solution process was chosen to be $n=10$. In order to facilitate computation, however, $n=5$ was taken for $p=0.004$ and other small values. All numerical results are believed to reproduce the behavior of the continuous wing with approximately ±1% accuracy.

Figure 3 summarizes the combined influences of drag and aspect ratio. (Care must be taken when interpreting the effect of changing p on the absolute level of flutter speed because of the manner in which this speed is nondimensionalized.) For the intermediate values of the other system parameters selected here, we see that it is on the larger-aspect-ratio wings that chordwise force makes itself felt. It is a curious fact, which we

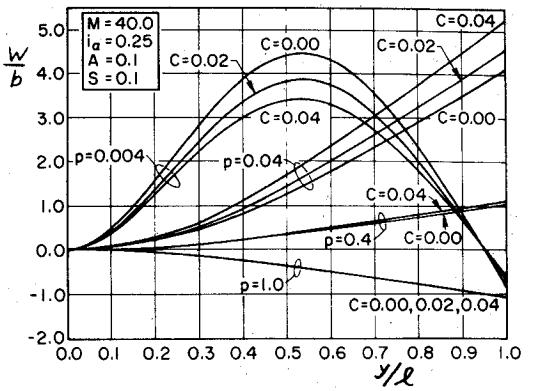

Fig. 5 Bending contribution to the mode shape of flutter, plotted vs dimensionless spanwise distance for several combinations of drag parameter C and aspect ratio parameter p.

are unable to explain physically, that for p between about 0.02 and unity increasing drag tends to increase flutter stability, whereas for the very slender wings with $p<0.02$ it is destabilizing. The sharp minimum near $p=1$ is, incidentally, believed to be associated with a familar phenomenon where uncoupled bending and torsional frequencies cross over one another.

An important question affecting the practical impact of the drag-flutter phenomenon on design is the relative magnitude of V and the speed V_D for static bending-torsion divergence of the same wing. It is a familiar fact of classical analysis that $V<V_D$ for most cantilevers. As the small selection of divergence entries in Table 1 suggests, however, the reverse easily can be true at the larger aspect ratios when drag is accounted for. Indeed, for the particular choice of parameters in Fig. 3, $V_D<V$ when p is less than roughly 0.05 and for both $C=0.02$ and 0.04. Other combinations can be found which render flutter more critical than divergence well into the range of aspect ratios where the influence of drag is unfavorable to both. Hence, each particular case must be examined for the role of each class of instability.

Whether the changes of order ±20% in flutter performance between $C=0$ and 0.04 carry any practical significance must be left to the reader's judgement. It is remarked, however, that the 2-5% unconservative error in a conventional flutter prediction might make the difference between meeting or failing to meet FAR or military specifications on flutter margin of safety, e.g., on a long-range cruising aircraft or sailplane wing with aspect ratio in the 10-20 range. A sudden pullup at high speed might be disastrous.

One finds no particular surprises when the roles of the other parameters in (24) are examined. For instance, the following typical behaviors can be inferred froms study of Table 1:

1) Increasing the density ratio M alone causes the flutter speed to rise approximately in proportion to $M^{1/2}$. This is a familar effect [cf., e.g., the discussion adjacent to Eq. (136), Ref. 3].

2) Increasing structural damping g tends to raise the speed by 1-2% throughout the parametric ranges in the table.

3) Increasing the mass moment of inertia i_α from 0.25 to 0.35 is stabilizing at high aspect ratio but destabilizing at low aspect ratio.

4) Doubling the mass unbalance S is destabilizing, except on the very stubby wings with $p=0.4$ and $A=0.2$.

5) Moving the elastic center aft by increasing A tends always to reduce the flutter speed markedly. At the higher aspect ratios, there is evidence that the (dimensionless) distance $S+A$ by which the sectional c.g. lies behind the aerodynamic center may be a more meaningful determinant of flutter performance than A or S separately. This is another familiar conclusion, and it seems unaffected when one accounts for drag.

Figures 4 and 5 are included to summarize some interesting discoveries regarding the mode shape at flutter and, by the way, to suggest why inaccuracies may occur when the motion is approximated by only one or two normal modes each for bending and torsion. In Fig. 4 the drag is zero, whereas parameter p ranges from 0.002 to nearly 2, with the other quantities in (24) having the indicated values. Small phase differences between spanwise stations are neglected. Each torsion mode in Fig. 4b is normalized to unit amplitude at the wingtip; the corresponding bending shapes have their values of w/b in proper proportion, save that the overall phase difference δ is not represented. We observe that torsion tends to occur almost purely in the fundamental, quarter-sine mode and that it is insensitive to large variations of the aspect-ratio parameter. On the other hand, the bending tends to be purely fundamental for p above 0.1, with its contribution nearly vanishing near 0.6. Below $p=0.1$, however, this mode makes a gradual transition toward a more complicated shape.

Figure 5 displays the influence of drag changes on the behavior detailed in Fig. 4a. Qualitatively the effects are not substantial. It is interesting, however, that increasing C_D depresses the peak bending amplitude where the flutter speed is being forced downward ($p+0.004$), and conversely at $p=0.04$.

V. Conclusions

By way of conclusion, we have attempted to show in a simplified fashion how chordwise force components can be included in the flexure-torsion flutter analysis of a cantilever wing. We make the point that, since drag never vanishes, it is a matter of consistency that some consideration should be given to its influence on the aeroelastic stability of systems like those we examine here. Using one, very elementary model wherein the chordwise force opposite to the flight direction is assumed constant in magnitude and uniform across the span, we predict that drag can depress the critical speed by up to 15% on very-large-aspect-ratio wings and increase it by a similar amount when the aspect ratio has an intermediate value. The combined effects of drag and other system parameters are displayed in Table 1.

We are the last to claim that a definitive study has been made of the phenomenon. Numerous aspects deserve further investigation, and we presently are looking at several. As for experimental verification, flutter tests from the 1940's and 1950's on large-aspect-ratio cantilevers might be reexamined to determine whether there is any systematic disagreement with theory which could be attributed to chordwise forces. Further analysis should introduce more realistic representations of drag, such as the follower force of the three-dimensional unsteady theory of Wagner.[2] T-tails and "cranked" wings have been pointed out to the authors as cases where drag might have an especially significant influence. Especially important is the question of high subsonic or supersonic flow, where much higher values of the parameter C will be encountered in practice than in the incompressible case.

References

[1] Petre, A., *Teoria Aeroelasticitatii—Statica,* Editura Academiei Republicii Socialiste Romania, Bucharest, 1966.

[2] Goetz, R.C., "Divergence of Some All-Movable Control Surfaces Including Drag Loadings," NASA TN D-4793, Oct. 1968.

[3] Bisplinghoff, R. L. and Ashley, H., *Principles of Aeroelasticity,* Wiley, New York, 1962.

[4] Wagner, S., "On the Singularity Method of Subsonic Lifting-Surface Theory," *Journal of Aircraft,* Vol. 6, Nov.-Dec. 1969, pp. 549-558.

[5] Garrick, I.E., "Propulsion of a Flapping and Oscillating Airfoil," NACA Rep, 567, May 1936.

[6] Petre, A., "L'effet de la Resistance a l'Avancement sur la Vitesse Critique du Flutter," *Proceedings of the Sixth International Congress of the Aeronautical Sciences,* Sept. 1968, Munich.

[7] Petre, A., "Non-Conservative Effects Produced by Thrust of a Jet Engine, Instability of Continuous Systems," *IUTAM Symposium Herrenalb,* 1969, Springer-Verlag, Berlin, 1971, pp 344-348.